

To appear in the Astrophysical Journal

Infrared Photometry of Starless Dense Cores

D.C. Murphy

Carnegie Institution of Washington, 813 Santa Barbara St., Pasadena, CA 91101

david@ociw.edu

P.C. Myers

Center for Astrophysics, 60 Garden St., Cambridge, MA

pmyers@cfa.edu

ABSTRACT

Deep JHK_s photometry was obtained towards eight dense molecular cores and $J - H$ vs. $H - K_s$ color-color plots are presented. Our photometry, sensitive to the detection of a $1 M_\odot$, 1×10^6 year old star through $\approx 35 - 50$ magnitudes of visual extinction, shows no indication of the presence of star/disk systems based on $J - H$ vs. $H - K_s$ colors of detected objects. The stars detected towards the cores are generally spatially anti-correlated with core centers suggesting a background origin, although we cannot preclude the possibility that some stars detected at H and K_s alone, or K_s alone, are not low mass stars or brown dwarfs ($< 0.3 M_\odot$) behind substantial amounts of visual extinction (e.g. 53 magnitudes for L183B). Lower limits to optical extinctions are estimated for the detected background stars, with high extinctions being encountered, in the extreme case ranging up to at least $A_V = 46$, and probably higher. The extinction data are used to estimate cloud masses and densities which are comparable to those determined from molecular line studies. Variations in cloud extinctions are consistent with a systematic nature to cloud density distributions and column density variations and extinctions are found to be consistent with submillimeter wave continuum studies of similar regions. The results suggest that some cores have achieved significant column density contrasts (~ 30) on sub-core scales (~ 0.05 pc) without having formed known stars.

Subject headings: stars: formation – ISM: clouds – ISM: globules

1. Introduction

The first near infrared (NIR, $\lambda = 1 - 2.5 \mu\text{m}$) observations of dark clouds were toward the Ophiuchus dark cloud complex by Grasdelen, Strom, and Strom (1973), who interpreted their observations as revealing the presence of an embedded star cluster. Pioneering studies such as this were hampered by their inability to distinguish between background field stars and embedded pre-main sequence (PMS) stars, as well as by their comparative lack of sensitivity compared with modern IR array based observations. Despite these problems, these initial surveys were able to detect small numbers of PMS objects in dark cloud regions, evaluate the reddening laws, and place lower limits on cloud dust extinctions. Visual extinctions for dark cloud complexes were typically found to be $\lesssim 10$ (Elias 1978a,b; Hyland 1981). Hyland (1981) reviewed the early work in this field and discussed the use of the $J - H$ vs. $H - K$ color-color plot as a powerful technique to discriminate PMS stars from field stars, laying the ground work for modern studies. The advent of NIR imaging brought a new impetus to NIR studies of dark clouds. Extensive surveys of cooler dust clouds, some known regions of low to intermediate mass star formation, have now been performed. These surveys have studied the embedded stellar content, probed the IMF, revealed the presence of brown dwarfs, and probed the mass distribution of molecular clouds (Evans 1999; Lada, Alves, and Lada 1999a; Lada 1998; Wilking 1997; Lada 1990). Recent studies by Hillenbrand et al. (1998) have shown that in Taurus-Auriga the $J - H$ vs. $H - K$ color-color plot method has an efficiency of 60% in identifying stars with optical signatures of accretion disks, whereas $H - K$ vs. $K - L$ color-color plots have an efficiency of 100%. Therefore, while the $J - H$ vs. $H - K$ color-color plot method probably cannot be taken as an absolute discriminant against the presence of star-disk systems, it still remains a powerful diagnostic for the presence of star-disk systems in a statistical sense. Also, in spite of these limitations, compared with longer wavelength IR observations, the NIR has numerous inherent practical advantages such as easier wide field coverage and ground based telescope aperture and accessibility with acceptably low sky/telescope background. The resilience of NIR photometry to reddening is also excellent, especially in the K_s passband ($\lambda = 2 - 2.35 \mu\text{m}$), where $A_K \simeq A_V/11$.

Most studies to date have concentrated on wide area, low sensitivity surveys of large star cloud molecular complexes or in some instances individual optically cataloged Bok globules, while fewer systematic surveys of dense molecular cores in the IR have been made. We present here the results of sensitive ($K_s \lesssim 17.2 - 19.8$) NIR observations of dense cores found in dark clouds. These cores are lacking in associations with optically identified young stellar objects or embedded IRAS sources.

An abundance of evidence now indicates that galactic star formation occurs in cold ($T = 10 - 20 \text{ K}$) dense ($n \geq 10^4 \text{ cm}^{-3}$) molecular cores either found as components of larger

molecular cloud complexes or as isolated dark clouds. Dense cores are identified by surveying these clouds in radio and millimeter spectral lines that trace dense molecular gas such as NH_3 and C^{18}O (Myers, Linke, and Benson 1983; Benson and Myers 1989). Clear evidence exists that these regions represent a link to the earliest stages of star formation. For instance, dense cores are often found in close proximity to groups of T-Tauri stars. More directly, some dense cores are known to have embedded young stellar objects (YSO's) or other indicators of embedded young stars. Star formation tracers associated with dense cores include Class 0 and I IRAS sources, HH objects, H_2O masers, several types of emission line stars (or other low-mass stars with extreme spectral features and colors), and bipolar gas flows (Beichman et al. 1986; Jijina, Myers, and Adams 1999). Naturally one is led to conjecture that dense cores represent an early stage of star formation: that of a self gravitating mass, portions of which are collapsing or have recently collapsed to form stars.

If such stars are undergoing gravitational collapse, the spectral signature for a line of modest optical depth ($\tau \sim 1$) is that of an apparent *blue-shifted profile* (Hummer and Rybicki 1968). Observations of YSO's and Class 0 IRAS sources (often associated with dense cores) have shown significant excess of blue-shifted spectral profiles indicating a significant population of sources with inward motions (Zhou et al. 1993, 1994; Myers et al. 1995; Gregerson et al. 1997; Mardones et al. 1997). Most YSO's are, however, also known to be associated with molecular outflows (bipolar flows), confusing the interpretation of spectral line data. Also, some observed inflows may not be truly "star forming" as most of the stellar mass might have already been accumulated.

The molecular cores selected for study here are a small and special subset of the cores from the lists of Benson and Myers (1989) and Lee, Myers, and Tafalla (2001) and are of special interest as candidates for the very earliest stage of low mass star formation. Specifically, these objects have been selected according to the following criteria:

- 1) They are free of known associations with optically visible PMS objects, and in fact most optically visible stars in their denser regions (as ascertained from Palomar Observatory Sky Survey Plates).
- 2) Most are not IRAS sources and have no other indicators of embedded star formation.
- 3) They have, in some cases, a spectral signature in millimeter wave transitions consistent with cloud gas infall. Five of the cores discussed here (L1689B, L183B, TMC1, TMC2, and L158) are classified as either "Strong Infall Candidates" or "Probable Infall Candidates" based a velocity analysis of extensive mapping in the $\text{CS}(2-1)$, $\text{N}_2\text{H}^+(1-0)$, and $\text{C}^{18}\text{O}(1-0)$ lines (Lee, Myers, and Tafalla 2001).
- 4) They are well studied at other wavelengths, are relatively nearby ($d \lesssim 450\text{pc}$), and

have projected molecular core sizes well matched to the \approx few arcminute scales of current NIR imaging cameras.

The objectives of our study here will be to:

1) Provide a further sensitive diagnostic of the embedded stellar or brown dwarf content of the dense cores allowing a less ambiguous interpretation of the gas velocity structure (i.e. infall vs. outflow) and clarifying the evolutionary state of these cores.

2) Measure the mass and density of the cores independent of methods based on molecular line observations which rely on numerous assumptions regarding molecule and grain chemistry, excitation physics, and radiative transfer.

3) Provide information on the spatial distribution and organization of the core gas in terms of central concentration and clumpiness.

2. Observations and data reduction

The observations were carried out in two observing runs at the 1 m Swope Telescope at Las Campanas Observatory, Chile, and one on the 60 inch telescope at Palomar Observatory. Infrared cameras utilizing the Rockwell NICMOS3 256 X 256 HgCdTe array were used. The camera used for the 60 inch telescope observations is an Offner reimager- based, all reflective design described in Murphy et al. (1995). The infrared camera used on the 1 m Swope telescope is also an Offner reimager camera, very similar in design to that described by Murphy et al. (1995), differing only in optical details primarily related to the fact that it is deployed on a telescope with a different focal ratio. The field-of-view (FOV) and plate scale of both cameras is nearly the same at 2.6' X 2.6' and 0.60" pixel⁻¹, respectively. Table 1 summarizes the observational parameters.

Frames at J , H , and K_s were obtained for all core positions, with typical integration times of several hundred seconds per filter, per core. The core positions (Table 2) were taken from the peaks of NH_2^+ and NH_3 emission line maps, both tracers of dense gas and velocity structure diagnostics. In the cases of L1709A and L1696B (which don't have published maps), the center of the IR frame is estimated to be approximately 50" east and 70" northeast of the published NH_3 positions, respectively, as these positions better define the overall the optical core. The final JHK_s images are elongated N-S from the intrinsic 2.6' X 2.6' camera fields by $\approx 10 - 40''$ as the telescope was dithered N-S a few times per color so that sky frames could be built from the data themselves as is standard with IR imaging. Twilight flats were taken at sunset and sometimes sunrise, and standard stars taken from Persson

et al. (1998) were systematically observed throughout the night. Darks were taken for all integration times used, usually at the beginning and end of the night, as well as during the night if time allowed (such as just after a standard star measurement). The seeing ranged from 0.9 - 2.0" (FWHM), depending on the telescope, site, airmass, and night, with typical values being close to 1" for the Las Campanas observations and 1.5" being typical for the poorer Palomar 60 inch site.

The data were reduced using IRAF and a standard set of scripts developed for this purpose at the Carnegie Observatories. All data frames were first linearized. Following this, all dark frames, and frames taken at the same position in the sky were averaged with a sigma clipping algorithm enabled to eliminate cosmic ray hits. Averaged dark frames were then subtracted from all data frames and the resultant dark-subtracted images were flat fielded using normalized twilight flats.

An iterative approach to sky subtraction was used to reduce the data. The point of the iterative operation is to suppress the residual stellar artifacts that would remain on a sky frame after conventional direct medianing, thus improving the accuracy of stellar photometry. Starting with the *dithered image frames* across each core position, i.e. linearized dark-subtracted flattened images, sky subtracted *final mosaics* were created by the following process. A median averaged sky frame was formed from all *dithered image frames*. This now star-free sky frame was further flattened with SExtractor to form a *first order sky* (Bertin and Arnouts 1996). This *first order sky* was subtracted from each *dithered image frame* to produce *reduced first order dither image frames*. Stars were then identified interactively on each of these *reduced first order dither image frames* and their (x, y) positions were logged to a disk file. The second iteration of the mosaic creation process begins by returning to the *dithered image frames* and using the saved (x, y) stellar positions to clean them of stars to form *star-free dithered image frames*. This second pass used a script based on the IRAF task imedit. The *star-free dithered image frames* were then medianed to obtain a *final sky* for each core at each color. Finally, the *final sky* was subtracted from the original *dithered image frames*, the resultant images were aligned and shifted using a fiducial reference star and sigma-clipped averaged to form a *final mosaic* at the core position. In a few cases the *final mosaic* was further processed by SExtractor to remove residual curvature.

To measure the magnitudes of the stars, the standards calibration was applied to each final mosaic, and aperture photometry performed by hand on individual stars using an IRAF script based on the IRAF *phot* routine. The brightest stars in a clean area of the frame were generally used to define the PSF for aperture photometry, although in cases where bright stars were not present, the PSF was determined from bright stars on the frames of other sources observed on the same night (at the same color). Aperture corrections to the

photometry of each star were estimated individually by graphically superimposing on the growth curve of every star the PSF. By shifting the PSF through a range of allowable fits, as determined by inspection, a range of possible aperture corrections was determined for every star. The errors in the photometry listed in Tables 3-10 are a quadrature combination of this full range, a statistical error due to photon noise on the mosaic, and a sigma determined from the set of all measurements of a standard star for that night. For faint stars, the errors are essentially dominated by the PSF fitting error, and for bright stars by the repeatable accuracy of measuring standard stars (since the bright stars all had well determined PSF's). The statistical sigmas determined from standards measurements are based on between 9 and 24 independent measurements per night, with an average of 13 measurements per night. These errors represent an absolute and well-determined floor to the photometric errors. For the fainter stars, we feel our error estimates tend to be on the generous side due to the approximate nature of our graphical fit and the fact that we roughly doubled the theoretical true error.

3. Results

The data are presented in the form of tables summarizing the photometry, processed images at each color, and $J - H$ vs. $H - K_s$ color-color diagrams.

Table 2 list the approximate center positions of the final image mosaics given in Figures 1-4 and their value in J2000.0 coordinates. The positional errors for the 1 m Swope observations ($\pm 10''$) are higher due to the poorer pointing accuracy of this telescope, and bearing in mind that optical reference stars in the fields are not available because of the generally star-free nature of the sources.

Tables 3-10 summarizes the photometry for each source. The columns give a running number identifying each star, the JHK_s magnitudes, $J - H$ and $H - K_s$ colors, and a reddening measure. Five sigma lower limits are estimated for each magnitude and color and are given in the table columns and are summarized in Table 11. To place these detection limits in a practical perspective, the last column Table 11 presents the visual extinction $A_V(lim)$ through which a $1 M_\odot$, solar abundance, 1×10^6 year old star should be detectable, assuming the core distances of Table 2, the reddening law of Koornneef (1983), and $M_J = 2.34$ (Siess, Dufour, and Forestini 2000).

In some cases the limiting magnitudes are fainter for redder colors despite the fact that observations at redder colors in the NIR are less sensitive due to higher background for the same integration time. This reversal of the normal state-of-affairs was due to the lack of

detectable stars at J or H , meaning that dithered frames could not be stacked together so that integration times at these bluer wavebands were less. Photometry and colors for a particular star are not given if for some reason a reliable value could not be obtained from the data, such as if the star is beyond or at the edge of the mosaic (specifically noted) or for any other reason a PSF fit could not be obtained (denoted by ellipsis in the table entries). The stars in Tables 3-10 are marked in Figures 1-4 on the image mosaic used for their identification, usually the K_s mosaic.

The last column of Tables 3-10, the reddening measure $A_V(K5)$, is an attempt to provide a relative measure of the core reddening. Calculated here is the optical extinction assuming that the typical background star is K5 main sequence (MS). Following the reddening law of Koornneef (1983), this is taken to be

$$A_V(K5) = 15.385E(H - K), \quad (1)$$

where $E(H - K)$ is the color excess given by

$$E(H - K) = (H - K) - (H - K)_{K5}. \quad (2)$$

Deriving $(H - K) = 0.16$ from Table 3 of Koornneef (1983), we obtain

$$A_V(K5) = 15.385[(H - K) - 0.160]. \quad (3)$$

This calculation is also performed for stars that have only $J - H$ lower limits and in such case would be a meaningful quantity if the star was field type as opposed to being a young star with a luminous disk embedded in the cloud. We note that the seemingly simplistic assumption that the typical background star is a K5 with $H - K = 0.16$ actually introduces a maximum error of only $\approx \pm 2.3$ magnitudes into the extinction estimate given by (3). This is because the intrinsic range of $H - K$ values for dwarfs and giants for spectral types A0 to M ranges only from 0.0 to 0.3 magnitudes (Koornneef 1983). A detailed discussion of this issue is given by Alves et al. (1998) and Lada et al. (1994). By way of example, these authors measured extinction free comparison fields for the dark clouds IC5146 and L977 yielding $H - K = 0.13 \pm 0.01$ and $H - K = 0.20 \pm 0.13$, respectively.

Figures 5-12 give $J - H$ vs. $H - K_s$ color-color plots for each core. The MS and reddening vectors of Koornneef (1983) are plotted on each diagram. Following Lada and Adams (1992) we have marked the reddened positions of stars projected off the MS at A_V 5, 10, 15, 20, 25, and 30 (where applicable) with X's. Lada and Adams (1992) provide a detailed observational and theoretical classification of YSO's in the $J - H$ vs. $H - K_s$ color-color plane. Lower limits (or in a few cases upper limits) on colors are indicated by arrows along the direction of the undetermined color. These are mostly lower limits on

$J - H$. In these plots, and all calculations, we have assumed that $K_s = K$ which will introduce a negligible error in our analysis, particularly in light of the other uncertainties in the photometry, reddening law, and intrinsic spectral nature of the detected stars (Persson et al. 1998; Rubio et al. 1998). The individual objects are discussed in detail in the following sections.

3.1. L1709A

Of the cores discussed here, L1709A had the most number of stellar objects detected in the IR: Colors or limits are presented for 39 stars in Table 3. Figure 1 displays the JHK_s mosaics and identifies the stars.

This core, despite its complete absence of optically identified stars on the digitized Palomar Observatory Sky Survey (POSS), exhibits stars in the infrared and shows an excess of stars with increasing infrared wavelength. The color-color plot Figure 5 indicates that nearly every star with plottable colors has colors consistent with being a reddened field star. The one possible exception is IR11 which is in a region of the color-color plot consistent with it being a classical T-Tauri star (CTTS) just slightly to the right of the reddened MS. We note that even this result is suspect since this data point has large error bars. The reddening measure (Table 3, col. 7) indicates that the L1709A stars range from unreddened to $A_V(K5) = 23.6$ with $\langle A_V(K5) \rangle = 12.2$.

3.2. L1582A

L1582A was the second most populous object in terms of the number of stars detected. Colors or limits are presented for 17 stars (Table 4). Figure 1 displays the JHK_s mosaics and identifies the stars.

As with L1709A, this core displays numerous visible IR stars increasing in number with wavelength, despite the fact that only two visible stars are detected on the POSS. The color-color plot Figure 6 indicates that all stars with plottable colors but one, IR5, have colors consistent with being field or reddened field stars. IR5 is in the classical T-Tauri star region (CTTS) of the color-color plot consistent with it being a young stellar object (Lada and Adams 1992). We note that this result is somewhat in doubt since this star is near the edge of the K_s frame, probably degrading the quality of the photometry. The reddening measure for L1582A (Table 4, col. 7) varies from $A_v = 1.5$ to 27.9.

3.3. L158

This core is devoid of stars on the POSS, but may be associated with the Class I IRAS source 16445-1352, located approximately 2' north of the molecular core center position and at the projected northern edge of the core. This IRAS source is $\approx 30''$ north of the northern boundary of our IR frame (Lee, Myers, and Tafalla 2001; Bontemps et al. 1996). Stars are seen in our NIR frame with colors or limits being provided for eight stars in Table 5. Figure 2 displays the JHK_s mosaic and identifies the stars.

The six plottable stars on the color-color diagram Figure 7 indicate field or reddened field stars except IR6 which displays colors consistent with it being a CTTS. We note however, that IR6 has very large error bars and is faint. Furthermore the $H - K_s$ error bar is nearly consistent with it being on the reddened main sequence. The JHK_s frames clearly show a greater visibility of stars with increasing wavelength. The reddening measure ranges from $A_V(K5) = 1.0$ to 34.3 (Table 5, col. 7).

3.4. TMC1

In the literature, TMC1 is often considered associated with the Class I IRAS 04381+2540 although we note that this object is 6' west and 1.8' north of the molecular core center position and well outside the boundary of our IR observations (Chandler, Barsony, and Moore 1998). Several stars are detected in our NIR frame, with colors or limits being given for given 11 stars in Table 6. Figure 2 displays the JHK_s mosaics and identifies the stars.

The nine plottable stars on the color-color diagram Figure 8 indicate that all stars have colors consistent with being highly reddened field stars although definitive statements cannot be made regarding stars with $J - H$ lower limits. The three stars found at the rightmost portion of the color-color diagram with $J - H$ lower limits are either highly reddened field stars, or PMS stars judging from the colors alone. The JHK_s images show a greater visibility of stars with wavelength, in fact only two stars had measurable J magnitudes. The reddening measures ranged from 12.6 to a remarkable 46.2, the greatest of all 67 extinction values reported in this paper.

3.5. L1696B

Colors or limits are presented for 12 stars towards the L1696B core (Table 7). Figure 3 identifies the stars and displays the H and K_s mosaics (no stars were detected at J).

Of the six plottable stars on the color-color diagram of Figure 9, two are clearly consistent with being field stars, while four are either very reddened stars or PMS objects judging from their colors alone. As is typical with all the cores, the images show a greater visibility of stars with wavelength. The reddening measures range from 18.4 to 36.0.

3.6. L134A

Colors or limits are presented for three stars towards the L134A core (Table 8). Figure 3 identifies the stars and display the H and K_s mosaics (no stars were detected at J).

All three stars are plotted on the color-color diagram Figure 10 as points with $J - H$ lower limits. Technically these are either PMS stars or highly reddened field stars. The reddening measures for these stars are 18.8, 16.5, 24.4.

3.7. TMC2

Colors or limits are presented for seven stars (Table 9) towards the TMC2 core. Figure 4 identifies the stars and displays the H and K_s mosaics (no stars were detected at J).

Only three of the stars were plottable on the color-color diagram (IR3, IR6, and IR7) and these only with $J - H$ lower limits making their nature uncertain (Fig. 11). The reddening measures for these stars are 33.9, 23.4, and 26.6 for IR3, IR6, and IR7, respectively.

3.8. L183B

Colors or limits are presented for three stars towards the L183B core (Table 10). Figure 4 identifies the stars and displays the H and K_s mosaics (no stars were detected at J).

Only one star (IR3) was plottable on the color-color diagram, and although it only has a $J - H$ lower limit, its colors are consistent with it being a reddened field star (Fig. 12). This core is the closest to being truly free of any associated stars of the sources studied here, displaying no detections at J and only one star in the H frame. IR3 has a reddening measure of 9.7.

4. Discussion

These dense cores, all initially considered to be nearly star-free in the optical and IRAS data, have in fact been shown to have numerous near infrared stellar detections projected near their centers. This result indicates the marginal utility of relying on survey optical plates to identify star-free dust clouds.

The color-color plots of these stars indicate, in the case where all three magnitudes are available, that nearly all have colors consistent with field stars, often highly reddened ones. Three stars discussed above have colors *possibly* consistent with an identification as PMS objects, but the evidence for this is very weak as these stars have, in all cases, arguably underestimated photometric errors. Reobservation of these stars, and if necessary, infrared spectroscopy on a large telescope could clarify this situation. There is no evidence of any substantial embedded stellar population in any of the sources (such as a star cluster).

There are many stars in our fields that are evident only at one or two colors (H and K_s), preventing their classification by use of the $J - H/H - K_s$ diagram. Our data do not allow us to make a definitive judgement as to the nature of these objects, although some useful constraints can be placed on their nature. As is evident from inspection of Figures 1-4, there is a clear tendency for *all* stars to be anti-correlated positionally with the core centers suggesting that all the detected stars are background stars. If any of the H and K_s only, or K_s only detected stars are core associated they are necessarily very young since statistical estimates of core lifetimes range from 0.3 - 1.6 Myr, and star formation and core dissipation times occur within a few crossing times (Elmegreen 2000; Lee and Myers 1999). If the one and two band detected objects are embedded star/disk systems, IRAS observations allow us to put some constraints on their properties. Assuming complete conversion of star/disk system photons into far infrared photons, and integrating the IRAS completeness limits (12 μm , 0.4 Jy), (25 μm , 0.5 Jy), (60 μm , 0.6 Jy), and (100 μm , 1.0 Jy) numerically between 12 and 100 μm , we obtain stellar luminosity detection thresholds of 0.043, 0.084, 0.12, and 0.69 L_\odot at 100, 140, 165, and 400 pc, respectively. These IRAS limits, taken from the IRAS explanatory supplement, are determined for galactic latitude $b > 50^\circ$ and may underestimate the true completeness limits since our cores are at lower galactic latitudes. The above luminosities convert approximately to stellar masses of 0.08, 0.11, 0.13, and 0.3 M_\odot assuming a 1×10^6 year old star, where the theoretical isochrones of D’Antona and Mazzitelli as presented in Wilking, Greene, and Meyer (1999), and Siess, Dufour, and Forestini (2000) have been used. Consider, for example a core at 100 pc, with a 1×10^6 year old 0.08 M_\odot star which would have an H absolute magnitude of ≈ 5.5 (Weintraub et al. 2000). Taking the H detection limit for L183B from Table 11, a distance modulus of 5, and the reddening law from Koornneef (1983), indicates that such a star would necessarily

suffer 53 magnitudes of visual extinction to evade detection at H . Such an extinction value, while quite high, is not precluded by our data.

The mean extinction measure as defined above is tabulated for each case in Table 12. To the extent that this measure indicates a reasonable indication of cloud optical extinction one can say that core extinctions range from 10 to about 30 magnitudes with a grand average of 19.4. The largest mean extinction was towards TMC1 (30.3), which also had the most reddened star IR7 with $A_V(K5) = 46.2$. Deeper and longer integrations on larger telescopes will be necessary to penetrate to the inner regions of these cores in the near infrared. These substantial extinctions clearly underestimate the true core extinctions, since, as is evident from the mosaic images in Figures 1-4, the detected stars strongly avoid the central regions of the cores. Our measured peak extinctions are a factor of ~ 10 higher than that determined by optical star counts of dark cloud regions and a factor of $\sim 2 - 4$ higher than that for the self gravitating, but non-starforming globule B68 recently surveyed to its core in the NIR (Alves, Lada, and Lada 2001; Cernicharo and Bachiller 1984). Furthermore, our extinctions tend to be slightly higher than the wide area NIR extinction surveys of IC5146 and L977 (Lada, Alves, and Lada 1999a). Our extinctions *are* generally comparable to, or less than absolute extinctions values found in starless prestellar cores from submillimeter-wave continuum surveys, consistent with the fact that our values are lower limits (Ward-Thompson, Motte, and Andre 1999; Visser, Richer, and Chandler 2001).

The IR data allows us to estimate a lower limit to the core densities for six cores where a clear boundary was defined on K_s images by the outermost stars. The area of a polygon formed by these stars was calculated using core distances taken from the literature (summarized in Table 2). The ordered star list forming the polygon boundary for each core is given in Table 13. The geometric core radius \sqrt{A} was divided into the core extinction measure from Table 12, and then multiplied by the standard factor of $0.95 \times 10^{21} \text{ cm}^{-2} \text{ mag}^{-1}$ (taking $A_V = 3.1E(B - V)$) to obtain an estimated lower limit on the total density of $\text{H}_2 + \text{H}$ (Bohlin, Savage, and Drake 1978). This method also allows a rough estimate on the core mass lower limit given by $n_{\text{tot}} A^{3/2} m_{\text{H}_2}$, where m_{H_2} is the mean mass of an H_2 molecule in the ISM, taken to be 2.3 times the mass of the hydrogen atom. The results of these calculations are given in Table 13. The densities, masses, and radii are all typical of dense cores in dark clouds. The density lower limit for L1582A is in agreement with the value of 1.6×10^4 of Jijina, Myers, and Adams (1999) determined from centimeter wave NH_3 inversion line data, while our density for L158 is an order of magnitude higher than the Jijina, Myers, and Adams (1999) value. Considering that our densities are lower limits, the L158 result is unlikely to be due to geometric uncertainties, suggesting a possible breakdown of NH_3 molecule as a probe of these high densities. Similar effects have been reported for C^{18}O , which is found to be correlated with A_V only up to $A_V \lesssim 10$ (Kramer et al. 1999).

Given the fact that we do not image all the way through the cores to background stars at K_s , it is reasonable to consider how likely a very faint low mass T-Tauri star or brown dwarf could, if located near the center of the cores, evade detection. In Table 14 we have calculated the faintest detectable absolute magnitude corresponding to a star or brown dwarf if located at the center of each core. To estimate M_J , this calculation assumes the reddening law of Koornneef (1983), extinctions to the centers of half the values given in Table 12, cloud distances from Table 2, and the detection limits from Table 11. Also given in Table 14 is M_{det} , an estimate of the mass of a star or brown dwarf corresponding to this M_J . These masses were taken from the evolutionary calculations given in Weintraub et al. (2000) assuming an upper limit of $\approx 1.6 \times 10^6$ yr for the star age based on core age estimates taken from Lee and Myers (1999). Considering that the hydrogen burning limit is about $0.08 M_\odot$, the results of this simple model indicate that in all cases except for L1696B our observations can plausibly rule out the presence of any low mass stars. In the case of L1696B, the model rules out the presence of all but the very faintest low mass stars just above the hydrogen burning limit. In the case of L1709A and L183B, brown dwarfs fainter than $0.01 M_\odot$ should be detectable, corresponding to objects of only 10 Jupiter masses. Our results are consistent with the findings of the recent VLA 3.6 cm survey of Harvey et al. (2002) which failed to detect embedded sources in four of our cores (TMC1, TMC2, L158, and L183) and placed upper limits of $\sim 0.1 L_\odot (d/140 \text{ pc})^2$ on the luminosities of embedded protostellar objects. We emphasize that our model results are somewhat tentative and will require deeper NIR observations as well as follow-up L band photometry to confirm.

The extinction estimates in Table 12 may in some cases underestimate the true core extinctions and that it is possible that a star or brown dwarf could "hide" on the far side of a core. For instance, Ward-Thompson, Motte, and Andre (1999) show that within a 13 arcsec beam, peak H_2 column densities implying extinctions ranging from $A_V = 61$ to $A_V = 232$ are found in prestellar dense cores similar to the sample studied here. On the other hand, the chance that an associated star could avoid detection is reduced if the associated star has an age in the middle of the likely range 0.3-1.6 Myr, discussed above, instead of the upper limit on age, 1.6 Myr, we adopted earlier. If the recent conjecture of Elmegreen (2000) is correct, that star formation time occurs in a crossing time, late-type deeply embedded stars would probably be $\approx 10^5$ yr in age otherwise core dissipation should have followed. Although the evolutionary calculations given in Weintraub et al. (2000) cut on at 1×10^6 yr, extrapolating from their Figure 5 (which plots M_J vs. age) indicates that for ages $< 1 \times 10^6$ yr significantly lower mass limits than given in Table 14 for L1709A, L1582A, TMC1, L134A, and L183B are indicated. This is a result of the expected sharply rising intrinsic luminosity of these objects with younger age.

The estimated individual stellar extinctions in Tables 3-10 show considerable scatter,

and generally speaking our data are too few to make detailed statements concerning the nature of the clumpiness of the extinguishing dust. This is natural of course as these sources were selected to be in star-free fields to begin with. For similar reasons it is not possible to make an estimate of cloud density profiles. However it is clear from Tables 3-10 and Figures 1-4 that column density contrasts ranging from ~ 1.5 - 34 exist in the clouds over scales of ~ 0.05 pc, comparable to submillimeter continuum results (Ward-Thompson, Motte, and Andre 1999; Visser, Richer, and Chandler 2001).

In order to ascertain if such column density variations are random in nature or a result of under sampling a systematic density profile, we can further analyze L1709A and L1582A, the two cores with enough stars to perhaps make statistical arguments plausible and ask if our results are consistent with the study of Lada, Alves, and Lada (1999b) (and references therein). These studies consider $\sigma_{A_V} - A_V$ correlations, where A_V is the mean optical extinction calculated from all stars in a given projected area, and σ_{A_V} is the standard deviation in A_V for all stellar values in that same area. This relationship can be used to distinguish the true nature of the underlying continuous extinction from undersampled data.

In an extensive study of the dark cloud IC 5146 employing ~ 2000 stars, Lada, Alves, and Lada (1999b) found a linear (σ_{A_V}, A_V) relationship. This relationship has a slope dependent on spatial filter size. Based on Monte Carlo density models constructed for IC 5146, Lada, Alves, and Lada (1999b) showed that a smoothly decreasing density distribution falling off as r^{-2} in a cylindrical cloud could explain the measured $\sigma_{A_V} - A_V$ relationships. The spatial filter size most relevant to our data is the $90''$ value since this covers the largest cloud fraction (IC 5146), as opposed to the same linear cloud size (our data sample is taken over the entire cloud). We note that at the distance of L1582A this $90''$ pixel is nearly the same linear dimension as in the Lada, Alves, and Lada (1999b) study since IC 5146 is at about the same distance (400pc). For this spatial filter, these authors obtained

$$\sigma_{A_V} \approx 1.0 + 0.41A_V. \quad (4)$$

Here σ_{A_V} is the mean standard deviation and A_V the mean optical extinction inside a $90''$ extinction map pixel. These authors do not give the error bars or intercepts of their fit for the $90''$ pixel case, so the intercept has been estimated from their Figure 10 and the intercept and slope errors are assumed similar to their equation 5, i.e. 0.11, and 0.01, respectively. A similar relation, but with a slope of 0.40 ± 0.02 and intercept 1.93 ± 0.11 , was obtained by Alves et al. (1998) for a sample of 1628 stars spanning a major fraction of the optically visible extinction towards the dark cloud L977. Applying the both the Lada, Alves, and Lada (1999b) and Alves et al. (1998) results to the $A_V(K5)$ values of Table 12 predicts $\sigma_{A_V} \approx 6.0 - 6.8$ for L1709A, and $\sigma_{A_V} \approx 5.6 - 6.4$ for L1582A. We calculate from all values in Tables 3 and 4, $\sigma_{A_V(K5)} = 5.9$ and $\sigma_{A_V(K5)} = 9.2$ for L1709A and L1582A, respectively.

Despite the considerable uncertainties in these comparisons, it is unlikely that the σ_{A_V} values derived from our data are the result of extinction due to either random clumpiness or a uniform smooth density distribution. For instance, if the extinction variation is due to completely random clumps in the line-of-sight, we would expect an approximately Poisson distributed distribution yielding $\sigma_{A_V(K5)} \approx [\langle A_V(K5) \rangle + \sigma_{obs}^2]^{1/2}$. Taking $\langle A_V(K5) \rangle$ values from Table 12 and a liberal estimation of $\sigma_{obs} = 2.3$ from section 3 above predicts $\sigma_{A_V(K5)} = 4.2$ and $\sigma_{A_V(K5)} = 4.1$ for L1709A and L1582A, respectively. On the other hand, if L1709A and L1582A were covered by a uniform veil of extinction with no density variation one would expect $\sigma_{A_V(K5)} \approx \sigma_{obs}$, yielding $\sigma_{A_V(K5)} \approx 2.3$ for L1709A and L1582A, respectively. Both these scenarios predict $\sigma_{A_V(K5)}$ values below those measured, particularly in the case of L1582A, tending to rule out these two possibilities.

5. Conclusions

We have studied eight dense cores with deep JHK_s photometry in the NIR, five of which exhibit extended "infall asymmetry" in the CS 2-1 millimeter wave transition (Lee, Myers, and Tafalla 2001). The main result of this study is, that based on the location of the detected stellar objects in the $J - H$ vs. $H - K_s$ color-color plane, there is no substantial evidence for an association of the cores with embedded star-disk systems. We note that while our observations are sensitive enough to detect a $1 M_\odot$, 1×10^6 year old star through $\approx 35 - 50$ magnitudes of optical extinction, the data show that we have not fully probed the core centers and a full census of the embedded star-disk system content will require both deeper NIR and longer wavelength IR observations. We note as well that although (as shown by Hillenbrand et al. (1998)) the $J - H$ vs. $H - K_s$ color-color plane method is a less than perfect diagnostic of the presence of star-disk systems, it should statistically reveal the presence of such systems if they are within our detection limits unless they are very rare. The cores are found to have mean extinction lower limits of between $A_V \approx 10 - 30$ with individual positions showing minimum extinctions as high as $A_V = 46$. The extinctions we measure are only lower limits and probably underestimate the true core extinctions. These extinctions are significantly higher than typical dark clouds or globules such as B68 determined either from optical or NIR surveys, but are consistent with submillimeter continuum surveys of starless cores. An analysis of individual cloud extinctions indicate column density contrasts of $\sim 1.5 - 34$ over scales of ~ 0.05 pc. A simple model suggests the cores may lack stellar objects down to at least the hydrogen burning limit in all cases except L1696B. This model result should be regarded as tentative since it is based on a variety of assumptions regarding the true core extinction, star ages, star cloud location, and the completeness of the $J - H$ vs. $H - K$ method as a diagnostic of embedded star-disk systems. Using the extinction data

we are able to estimate core densities and masses and have found them to be consistent with estimates determined from radio molecular line observations. A statistical analysis of the variation in extinction for L1709A and L1582A as characterized by $\sigma_{AV(K5)}$ is inconsistent with either a random or uniform density structure and may suggest a smoothly varying systematic density distribution.

We thank Chang Won Lee for assistance with the observations. We thank the staffs of Las Campanas and Palomar observatories for their assistance. We thank Eric Persson for supplying the data reduction scripts and providing invaluable advice on the data reduction process. Phil Myers gratefully acknowledges support from NASA grant NAG5-6266.

REFERENCES

- Aspin, C., Sandell, G., and Russell, A.P.G. 1994, A&AS, 106, 165
- Alves, J., Lada, C.J., and Lada, E.A. 2001, Nature, 409, 159
- Alves, J., Lada, C.J., Lada, E.A., Kenyon, S.J., Phelps, R. 1998, ApJ, 506, 292
- Beichman, C.A., Myers, P.C., Emerson, J.P., Harris, S., Mathieu, R., Benson, P.J., and Jennings, R.E. 1986, ApJ, 307, 337
- Benson, P.J., and Myers, P.C. 1989, ApJS, 71, 89
- Bertin, E., and Arnouts, S. 1996, A&AS, 117, 393
- Bohlin, R.C., Savage, B.D., and Drake, J.F. 1978, ApJ, 224, 132
- Bontemps, S. Andre, P., Terebey, S., and Cabrit, S., A&A, 311, 858
- Cernicharo, J., and Bachiller, R. 1984, A&AS, 58, 327
- Chandler, C.J., Barsony, M., and Moore, T.J.T. 1998, MNRAS, 299, 789
- Elias, J.H. 1978, ApJ, 224, 453
- Elias, J.H. 1978, ApJ, 224, 857
- Elmegreen, B.G. 2000, ApJ, 530, 277
- Evans, N.J. 1999, ARA&A, 37, 311

- Grasdelen, G.L., Strom, K.M., and Strom, S.E. 1973, *ApJ*, 184, L53
- Gregerson, E.M., Evans, N.J., Zhou, S., and Choi, M. 1997, *ApJ*, 484, 256
- Harvey, D.W.A., Wilner, D.J., Di Francesco, J., Lee, C.W., Myers, P.C. 2002, *AJ*, 123, 3325
- Hillenbrand, L.A., Strom, S.E., Calvet, N., Merrill, K.M., Gatley, I., Makidon, R.B., Meyer, M.R., and Skrutskie, M.F. 1998, *ApJ*, 116, 1816
- Hyland, A.R. 1981, A.R., in *IAU Symposium No. 96, Infrared Astronomy*, ed. C.G. Wynn-Williams and D.P. Cruikshank (Dordrecht: Reidel), 125
- Hummer, D., and Rybicki G.B. 1968, *ApJ*, 153, L107
- Jijina, J., Myers, P.C., and Adams, F.C. 1999, *ApJS*, 125, 161
- Kramer, C., Alves, J., Lada, C.J., Lada, E.A., Sievers, A., Ungerechts, H., and Walmsley, C.M. 1999, *A&A*, 342, 257
- Koornneef, J. 1983, *A&A*, 128, 84
- Lada, E.A. 1990, Ph.D. Thesis, The University of Texas, 1990
- Lada, C.J., and Adams 1992, F.C. 1992, *ApJ*, 393, 278
- Lada, E.A. 1998, in *Origins*, ASP Conference Series, 148, 198
- Lada, C.J., Alves, J., and Lada, E.A. 1999, in *The Physics and Chemistry of the Interstellar Medium*, Proceedings of the 3rd Cologne-Zermatt Symposium, ed. V. Ossenkopf and G. Winnewisser, GCA-Verlag Herdecke, 161
- Lada, C.J., Alves, J., and Lada, E.A. 1999, 512, 250
- Lada, C.J., Lada, E.A., Clemens, D.P., and Bally, J. 1994, *ApJ*, 429, 694
- Lee, C.W., and Myers, P.C., F.C. 1999, *ApJS*, 123, 233
- Lee, C.W., Myers, P.C., and Tafalla, M. 2001, *ApJS*, 136, 703
- Mardones, D., Myers, P.C., Tafalla, M., Wilner, D.J., Bachiller, R., and Garay, G. 1997, *ApJ*, 489, 719
- Mattila, K. 1986, *A&A*, 160, 157
- Murphy, D.C., Persson, S.E., Pahre, M.A., Sivaramakrishnan, A., and Djorgovski, S.G. 1995, *PASP*, 107 1234

- Myers, P.C., Linke, R.A., and Benson, P.C. 1983, *ApJ*, 264, 517
- Myers, P.C., Bachiller, R., Caselli, P., Fuller, G.A., Mardones, D., Tafalla, M., and Wilner, D.J. 1995, *ApJ*, 449, L65
- Persson, S.E., Murphy, D.C., Krzeminiski, W., Roth, M., and Rieke, M.J. 1998, *AJ*, 116, 2475
- Rubio, M., Barba, R.H., Walborn, N.R., Probst, R.G., Garcia, J., and Roth, M.R. 1998, *AJ*, 116, 1708
- Visser, A.E., Richer, J.S., and Chandler, C.J. 2001, *MNRAS*, 323, 257
- Siess, L., Dufour, E., and Forestini, M. 2000, *A&A*, 358, 593
- Ward-Thompson, D., Motte, F., and Andre, P. 1999, *MNRAS*, 305, 143
- Weintraub, D.A., Saumon, D., Kastner, J.H., Forveille, T. 2000, *ApJ*, 530, 867
- Wilking, B.A. 1997, in *Origins of Life and Evolution of the Biosphere*, 27, Issue 1/3, 135
- Wilking, B.A., Greene, T.P., and Meyer, M.R. 1999, *ApJ*, 117, 469
- Zhou, S., Evans, N.J., Kompe, C., and Walmsley, C.M. 1993, *ApJ*, 404, 232
- Zhou, S., Evans, N.J., Peng, R., and Lo, K.Y. 1994, *ApJ*, 433, 131
- Zinnecker, H., McCaughrean, M. 1991, *Mem. Soc. Astron. It.*, 62, 761

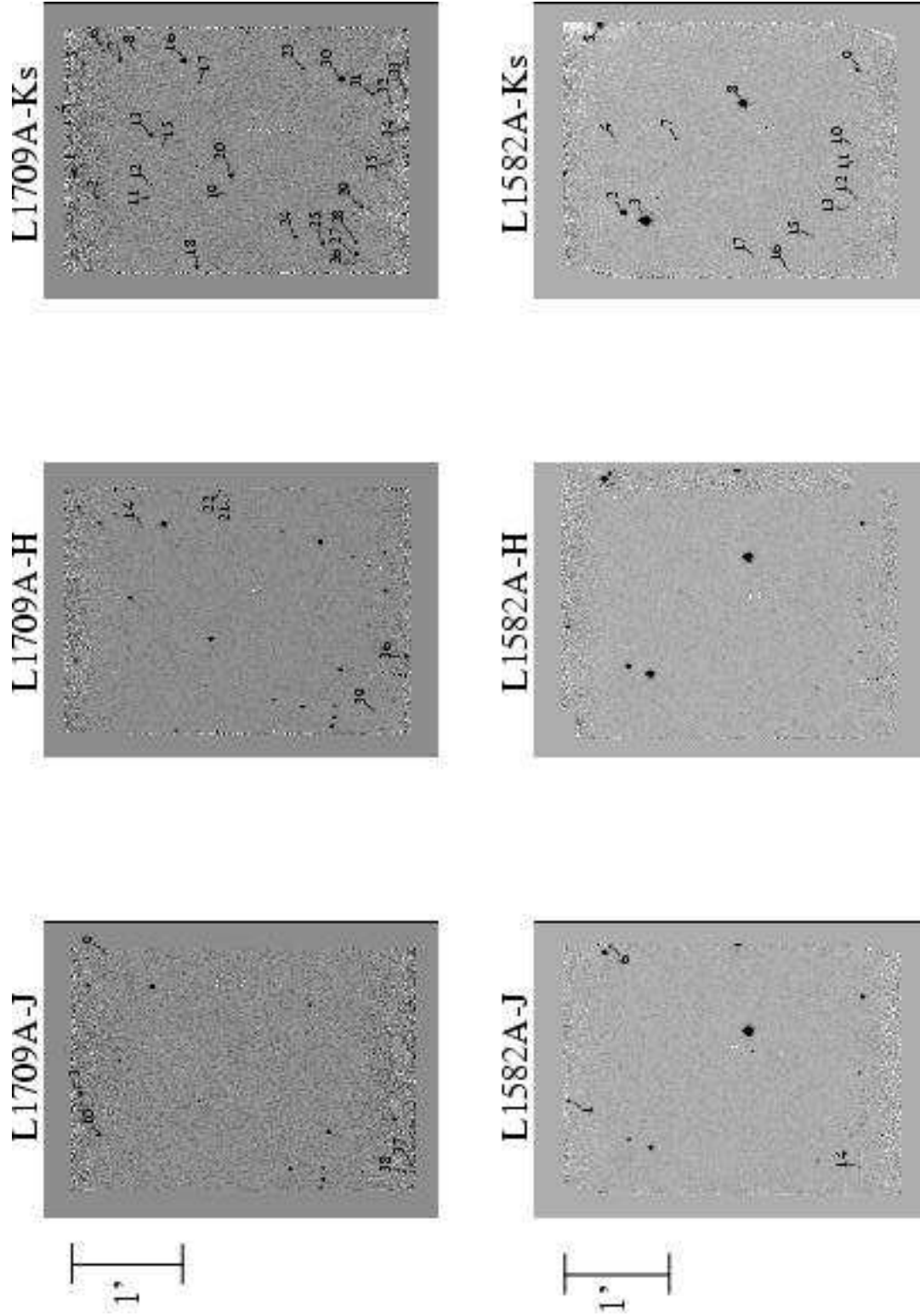


Fig. 1.— JHK_s mosaics of L1709A and L1582A

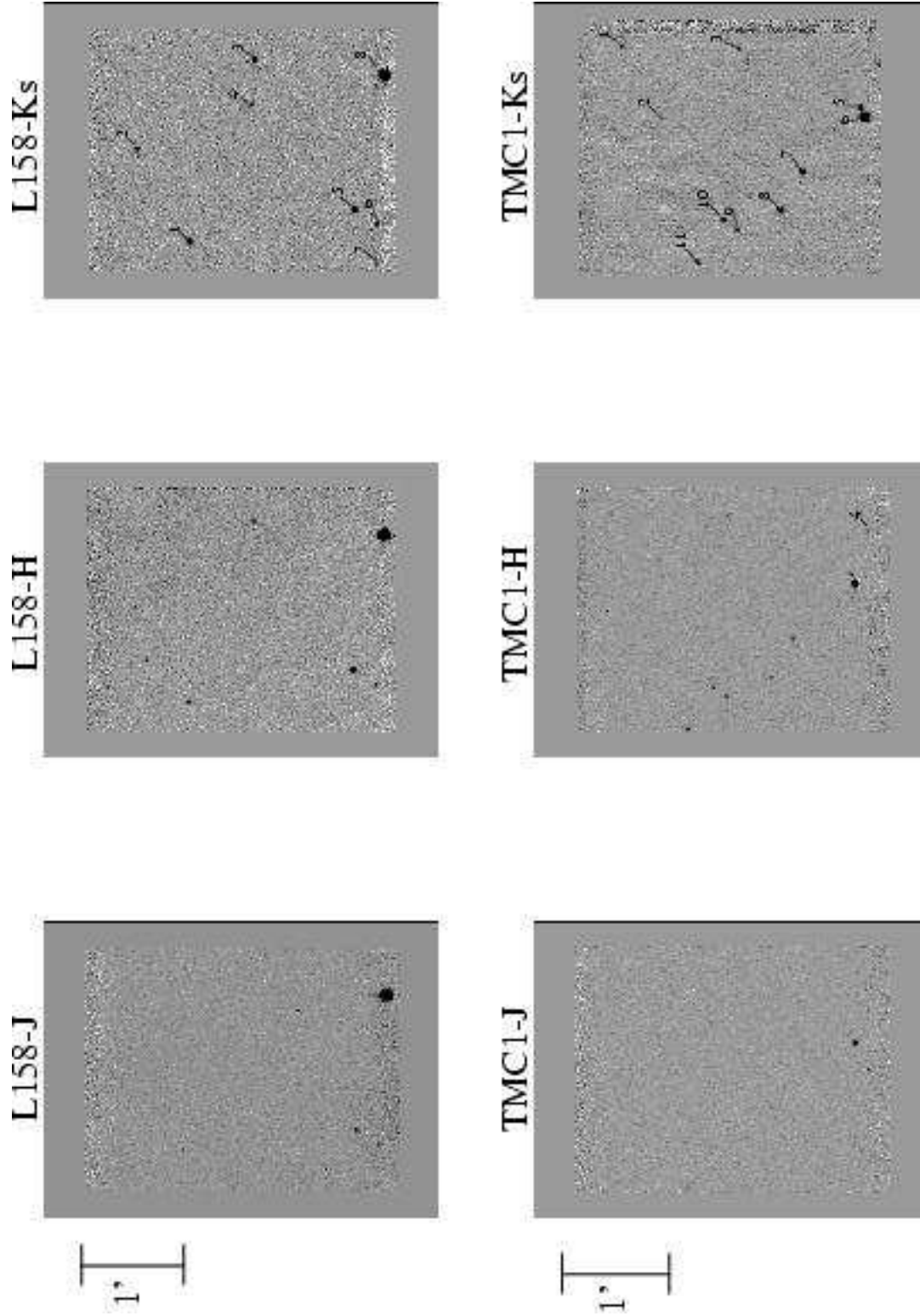


Fig. 2.— JHK_s mosaics of L158 and TMC1

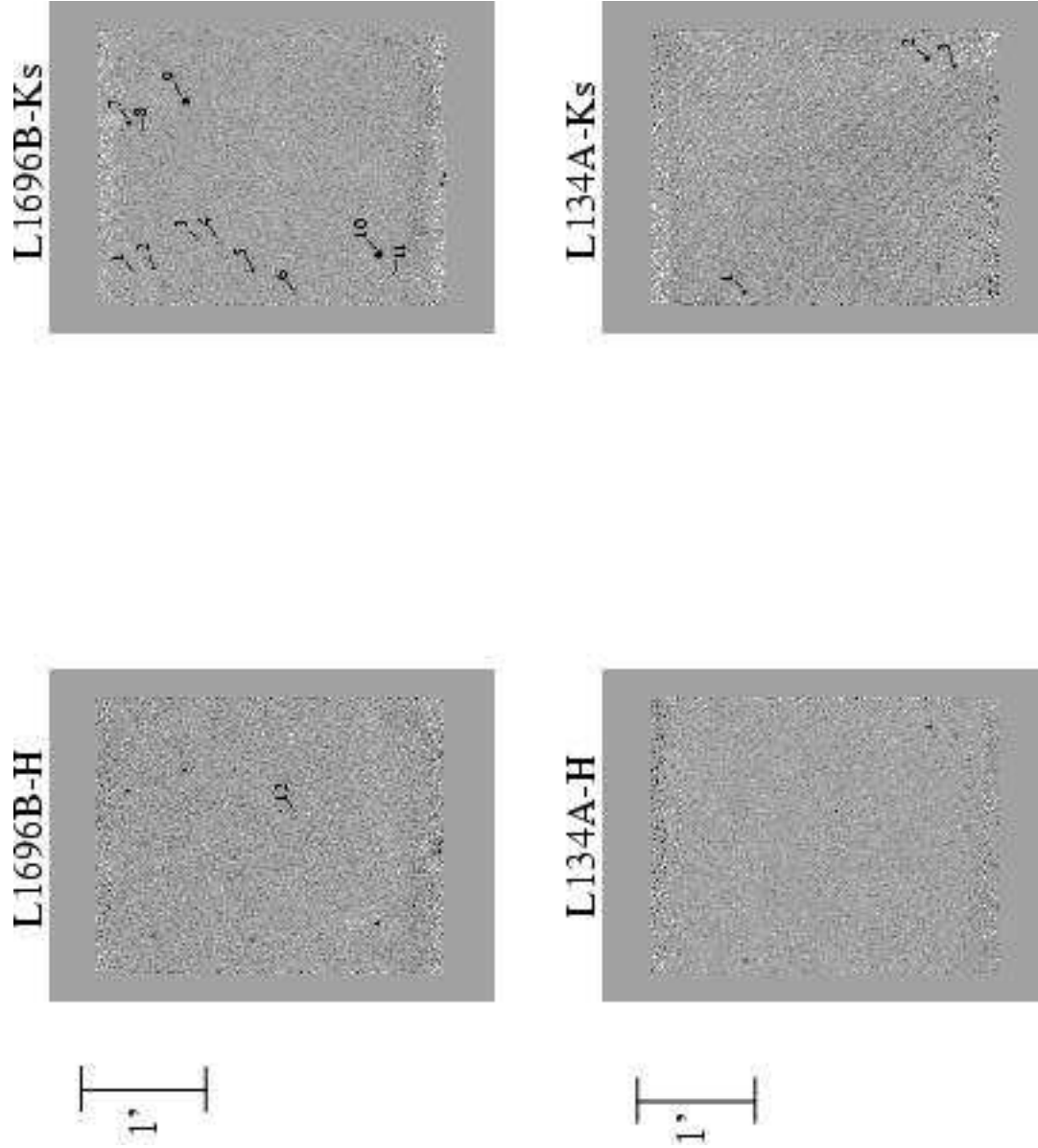


Fig. 3.— HK_s mosaics of L1696B and L134A

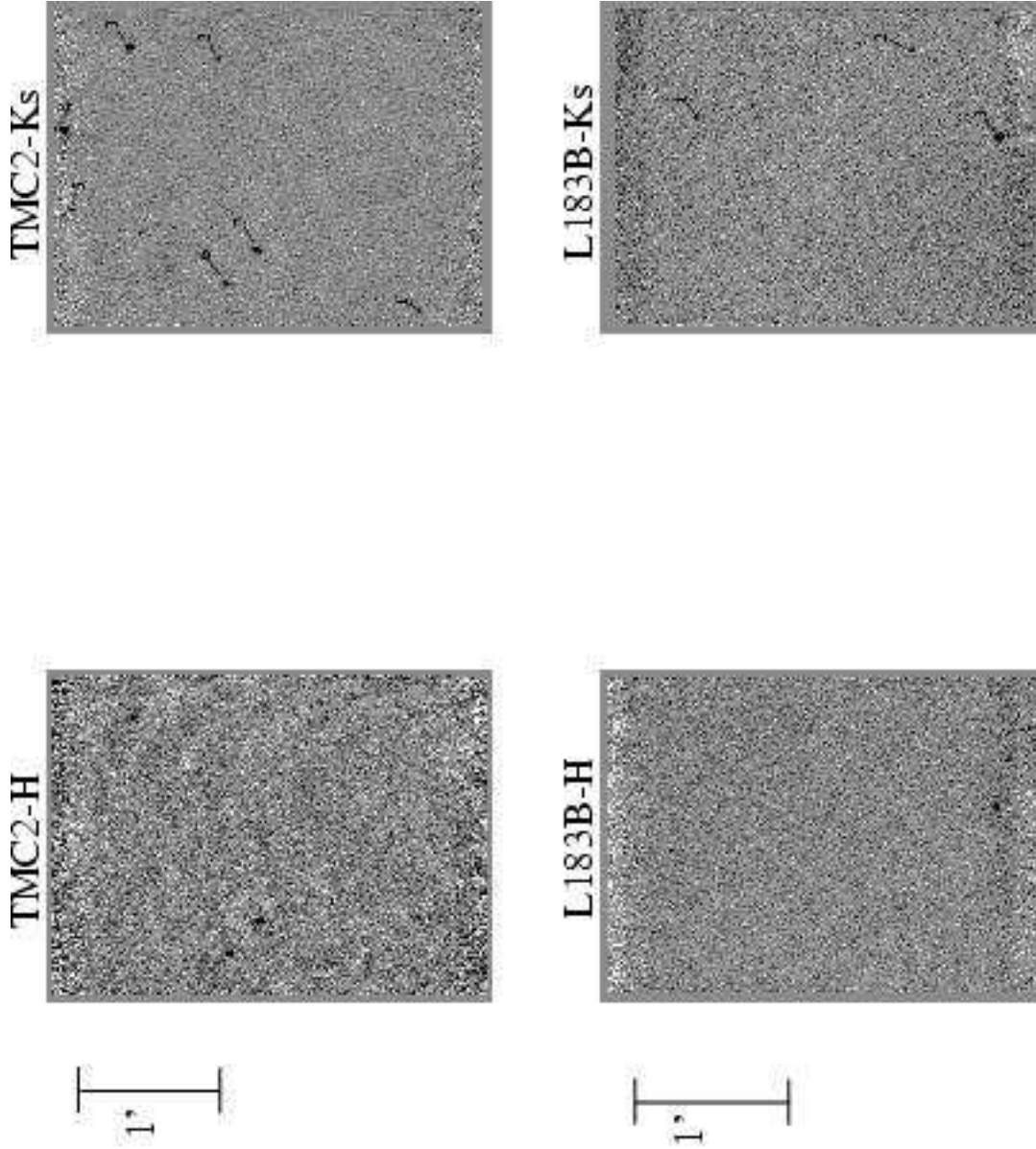


Fig. 4.— HK_s mosaics of TMC2 and L183B

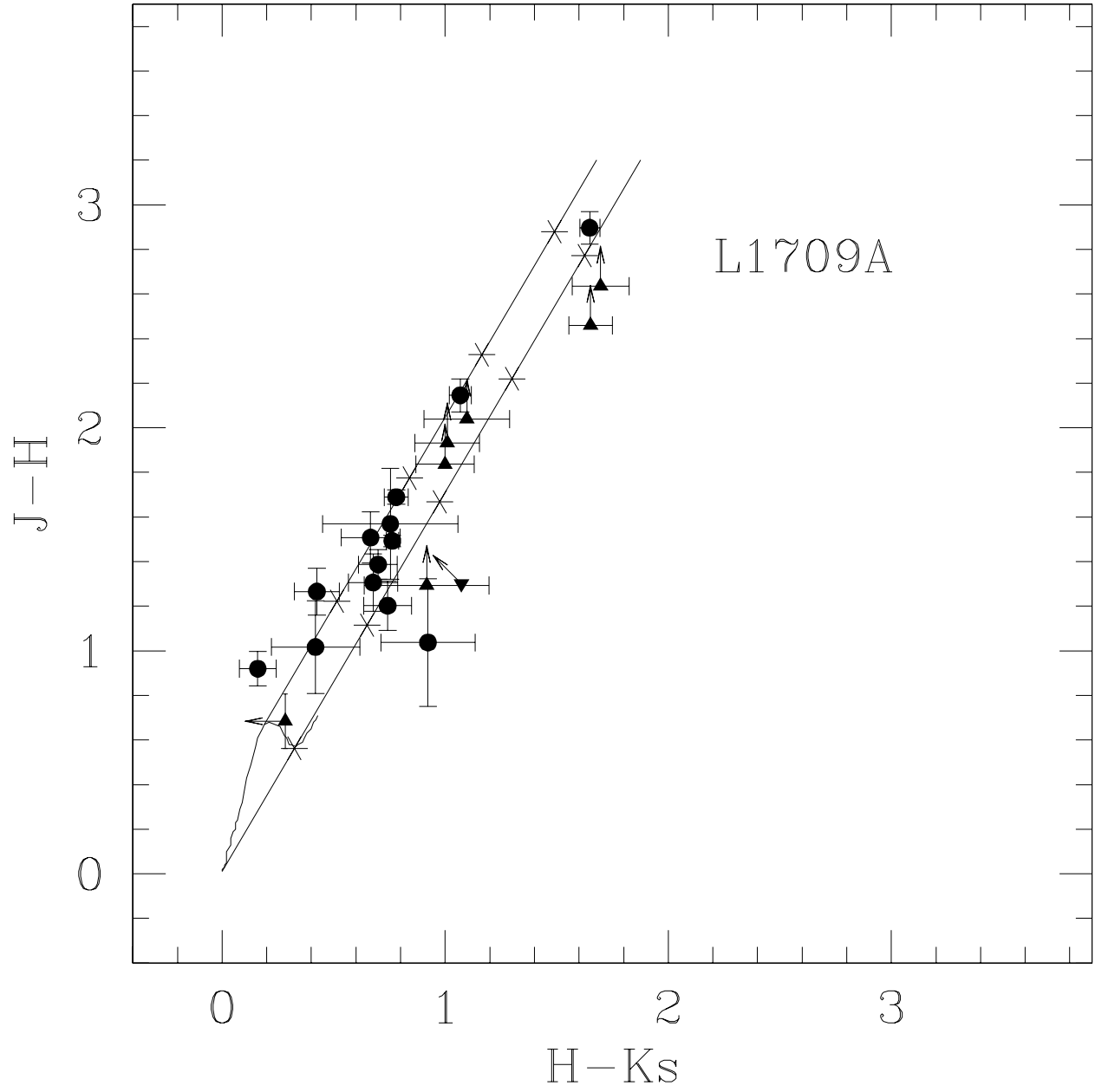


Fig. 5.— Color-color plot for L1709A.

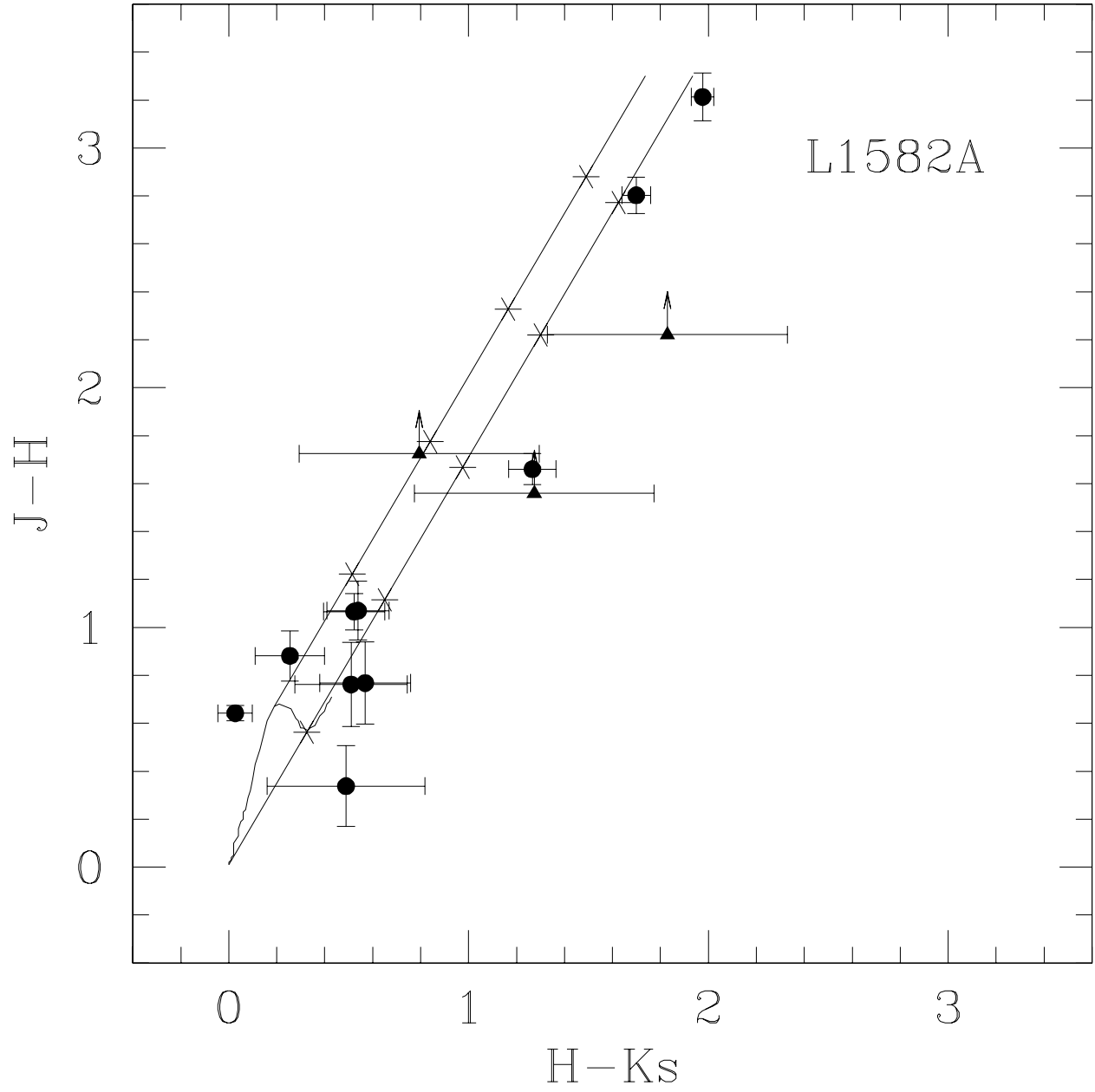


Fig. 6.— Color-color plot for L1582A.

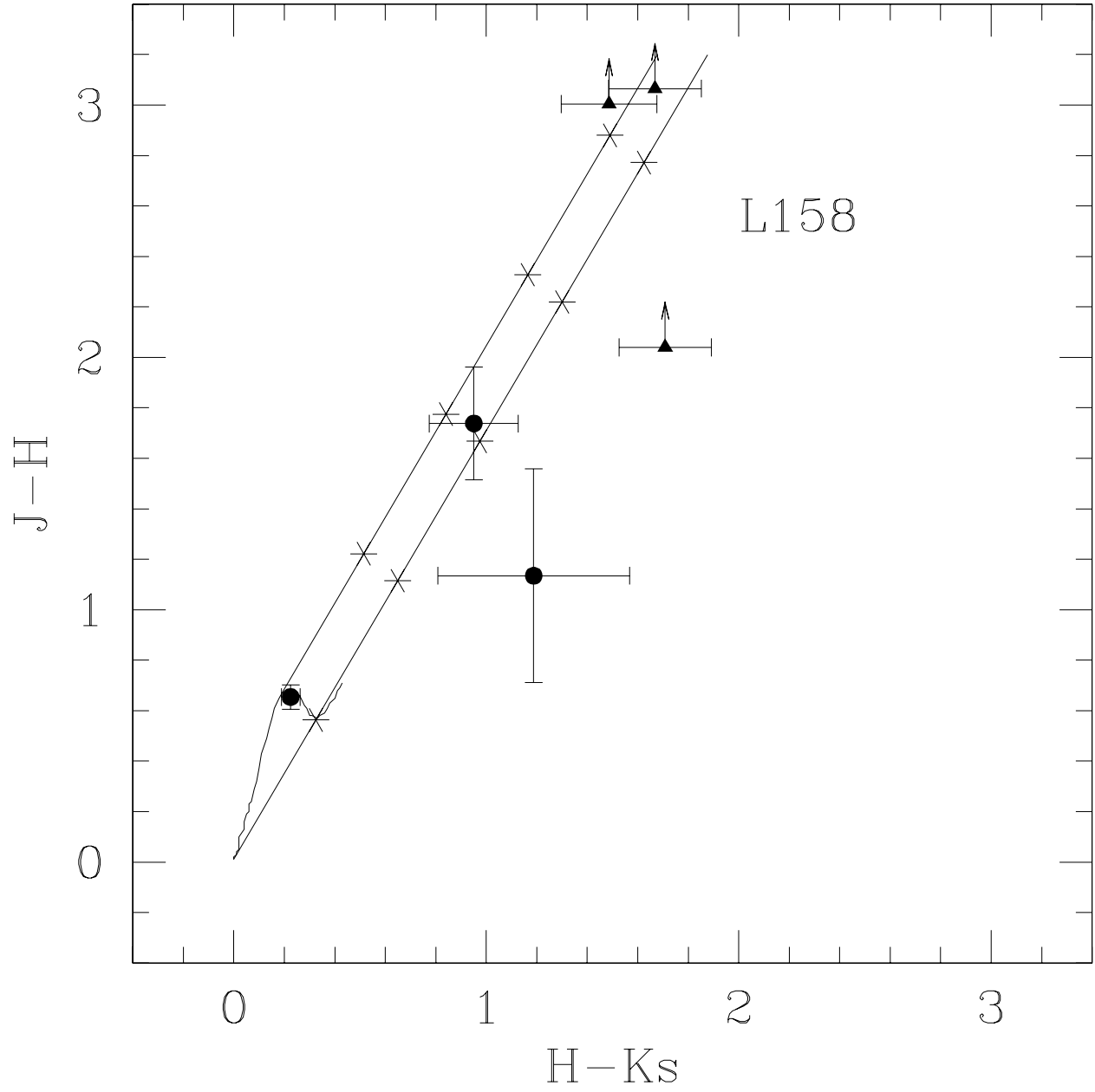


Fig. 7.— Color-color plot for L158.

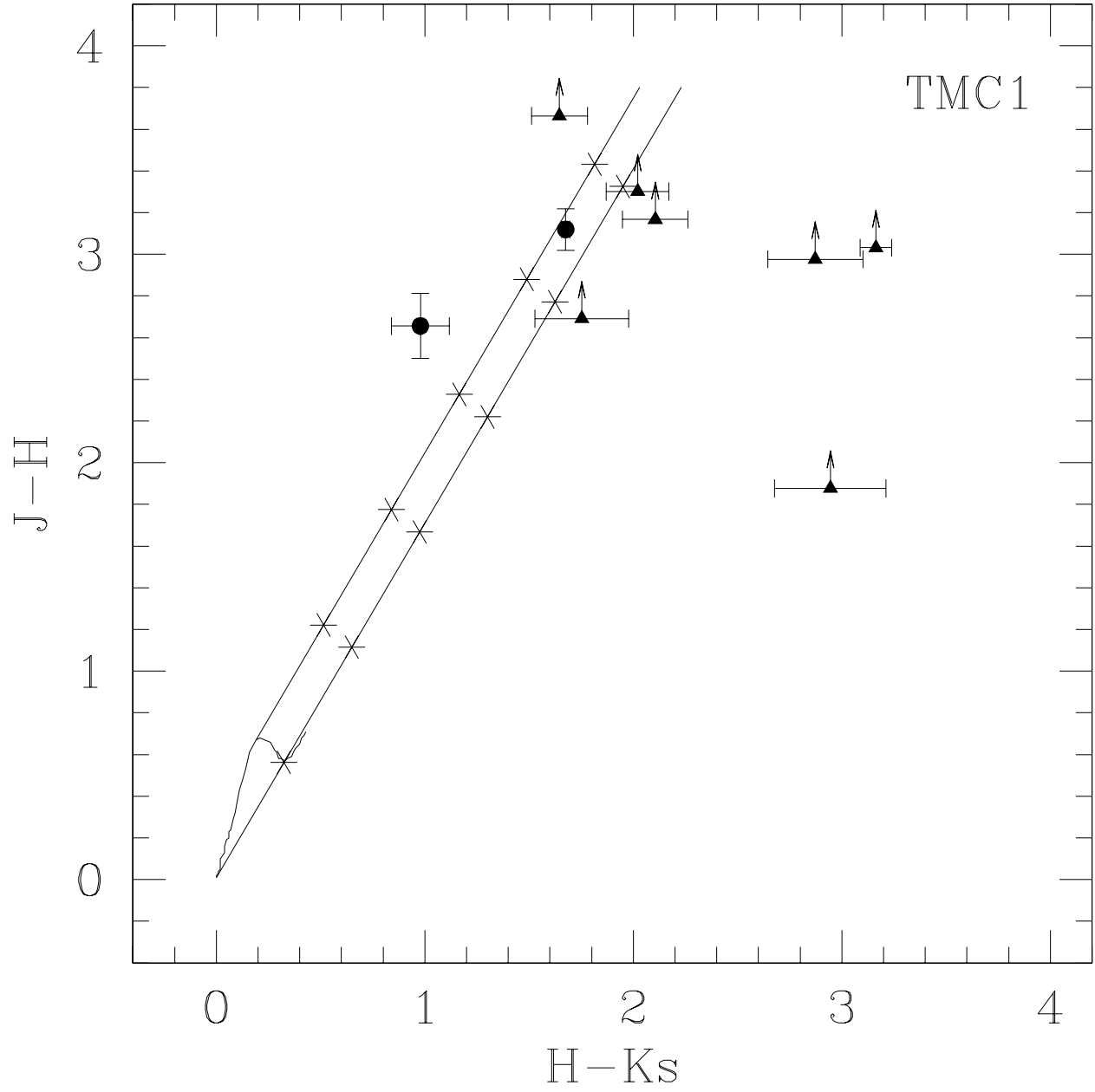


Fig. 8.— Color-color plot for TMC1.

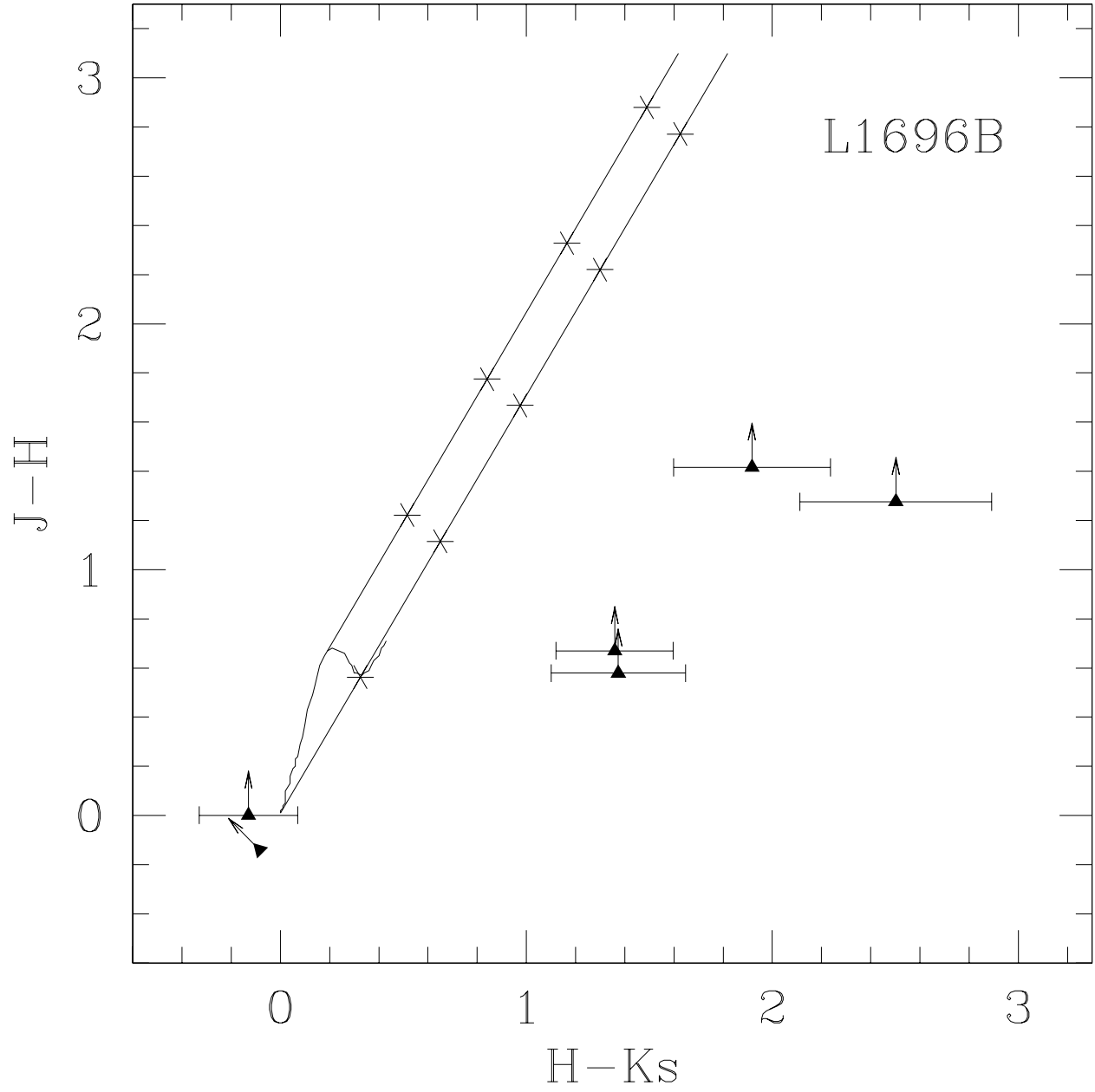


Fig. 9.— Color-color plot for L1696B.

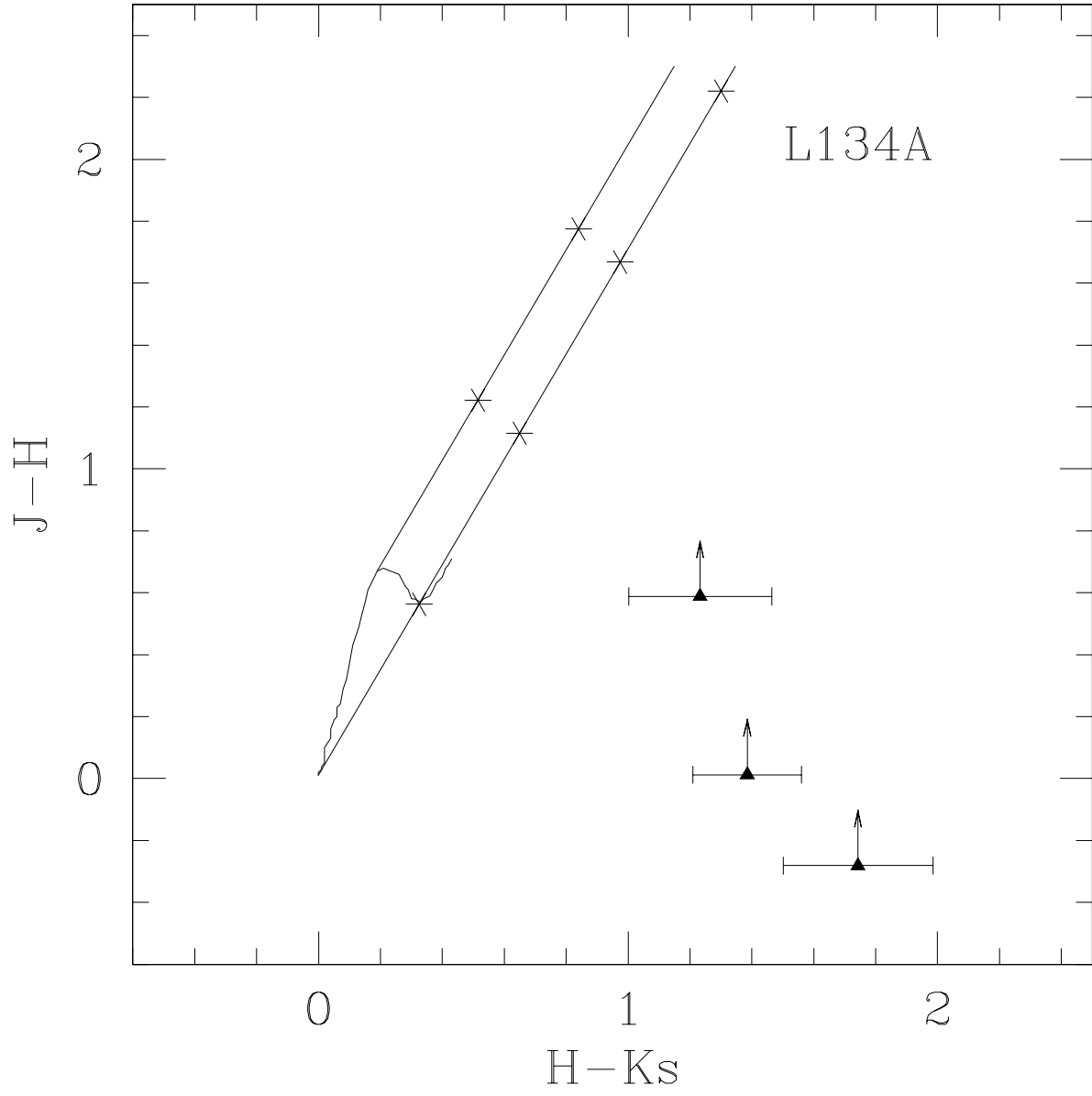


Fig. 10.— Color-color plot for L134A.

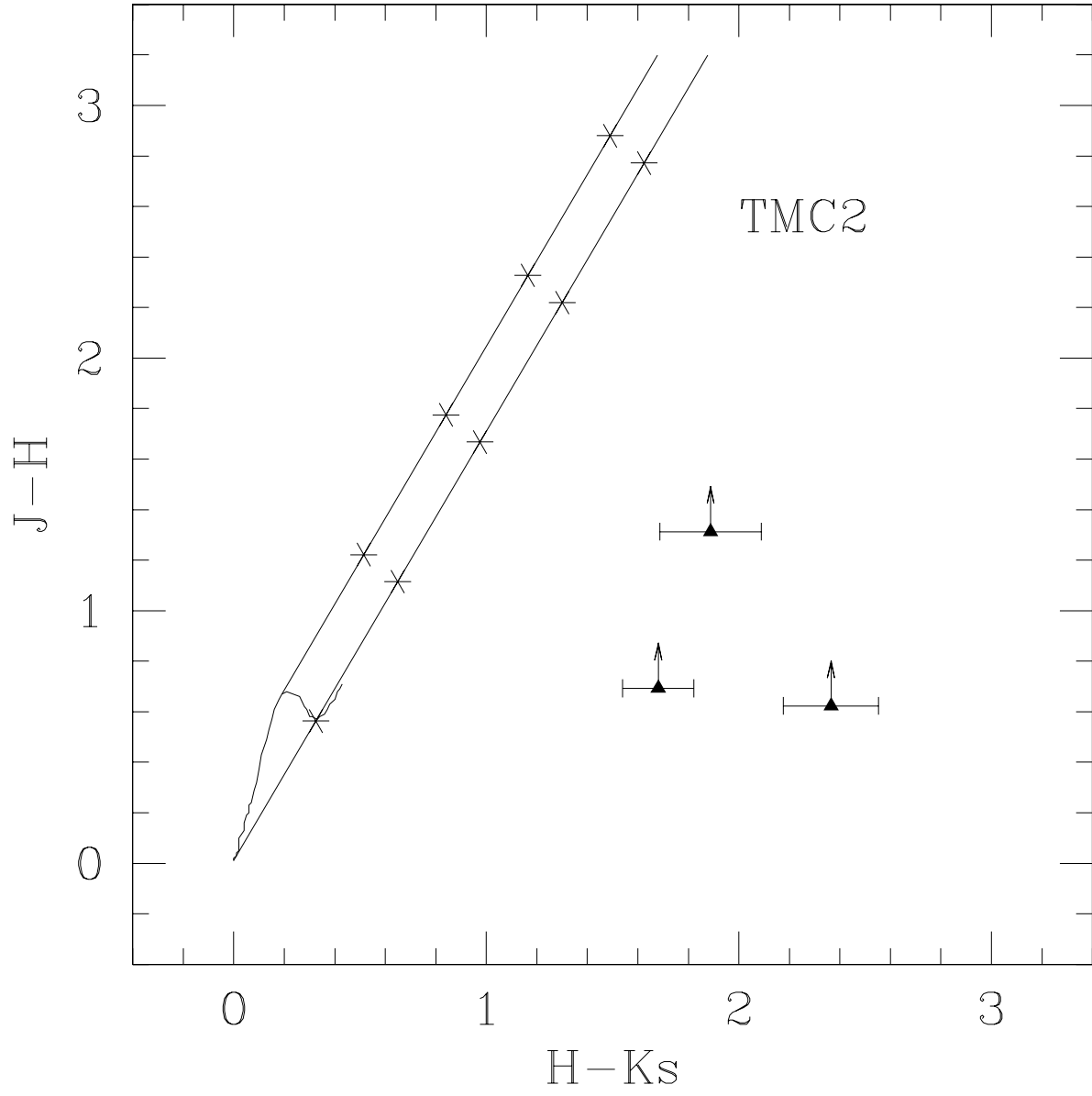


Fig. 11.— Color-color plot for TMC2.

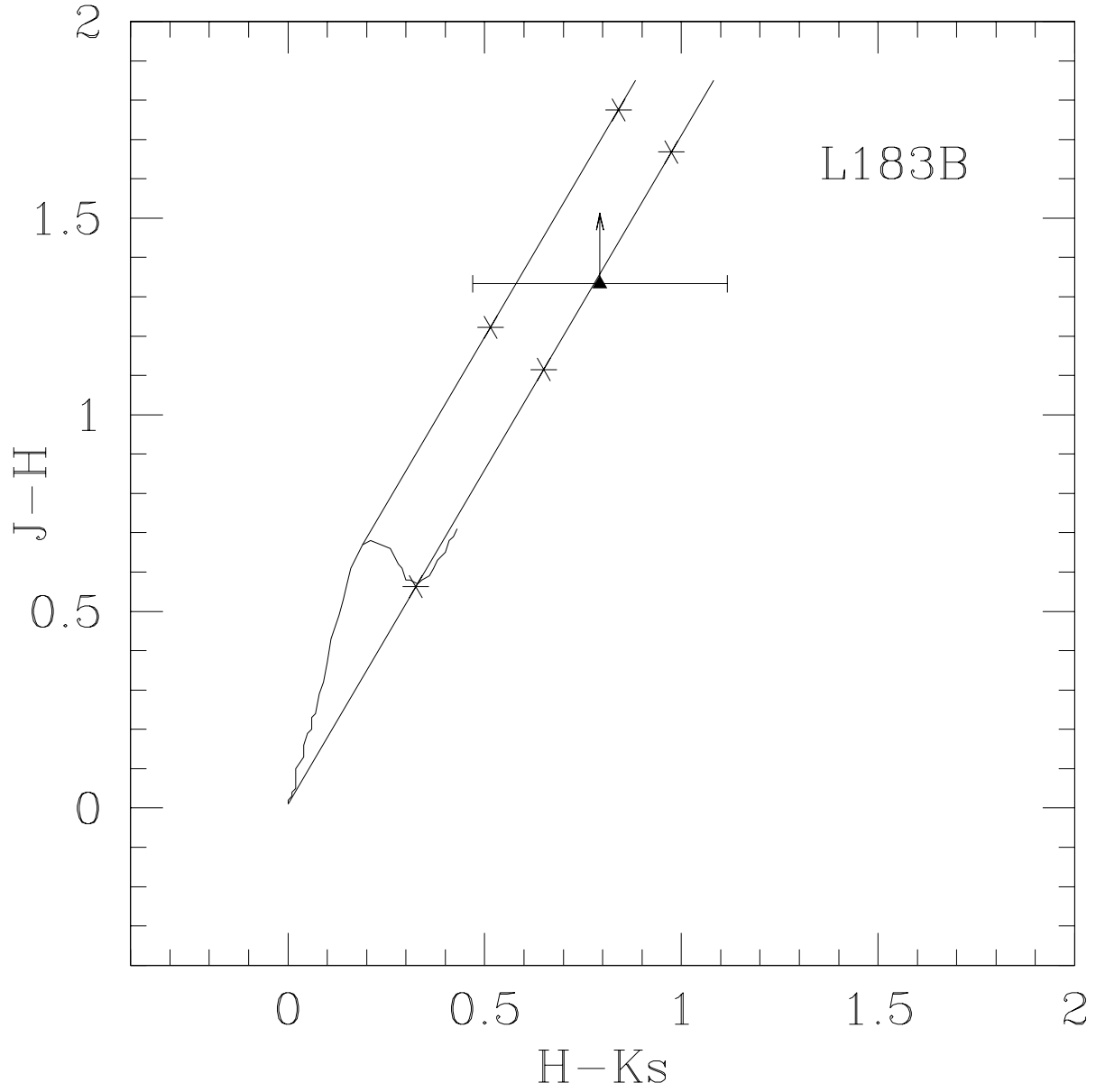


Fig. 12.— Color-color plot for L183B.

Table 1. Observational parameters.

Run	UT Dates	Telescope	Camera Plate Scale (arcsec pixel ⁻¹)	Camera FOV (arcmin)
1	6/17/97 - 6/23/97	LCO 1 m	0.60	2.56 X 2.56
2	11/6/97 - 11/8/97	Pal 1.5 m	0.62	2.65 X 2.65
3	3/17/98 - 3/19/98	LCO 1 m	0.60	2.56 X 2.56

Table 2. Starless dense core field centers and distances.

Core Name	R.A. (J2000.0)	Decl. (J2000.0)	Est. Pos. Error (arcsec)	Position Reference	Distance (pc)	Distance Reference	Run
L1709A	16 30 50.8	-23 41 53.0	± 10	a	165	c	3
L1582A	5 32 00.3	12 30 28.2	± 10	a	400	c	3
L158	16 47 23.2	-13 59 21.1	± 10	a	165	c	1
TMC1	4 41 33.0	25 44 44.0	± 5	b	140	d	2
L1696B	16 28 59.3	-24 20 43.0	± 10	a	165	c	1
L134A	15 53 36.4	-4 35 26.0	± 10	a	100	e	1
TMC2	4 32 48.7	24 25 12.0	± 5	b	140	c	2
L183B	15 54 06.5	-2 51 39.0	± 10	b	100	e	1

^aBenson and Myers (1989). Also, see text.

^bLee, Myers, and Tafalla (2001)

^cLee and Myers (1999)

^dJijina, Myers, and Adams (1999)

^eMattila (1986)

Table 3. Magnitudes and colors for identified L1709A stars.

Star	J	H	K_s	$J - H$	$H - K_s$	$A_V(K5)$
1	off frame	off frame	15.037 ± 0.090
2	off frame	17.752 ± 0.133	16.660 ± 0.354	...	1.092 ± 0.378	14.339
3	17.692 ± 0.065	> 19.262	> 17.868	< -1.570
4	off frame	off frame	15.402 ± 0.106
5	off frame	off frame	16.818 ± 0.166
6	off frame	16.990 ± 0.127	16.346 ± 0.109	...	0.644 ± 0.167	7.446
7	17.626 ± 0.042	16.360 ± 0.096	15.935 ± 0.032	1.266 ± 0.105	0.425 ± 0.101	4.077
8	19.172 ± 0.160	18.155 ± 0.133	17.736 ± 0.147	1.017 ± 0.208	0.419 ± 0.198	3.985
9	18.741 ± 0.092	17.425 ± 0.113	off frame	1.316 ± 0.146
10	17.937 ± 0.145	> 19.262	> 17.868	< -1.325
11	19.783 ± 0.244	18.746 ± 0.149	17.823 ± 0.149	1.037 ± 0.286	0.923 ± 0.211	11.739
12	20.157 ± 0.235	18.588 ± 0.082	17.834 ± 0.149	1.569 ± 0.249	0.754 ± 0.304	9.139
13	17.781 ± 0.047	16.394 ± 0.048	15.695 ± 0.073	1.387 ± 0.067	0.699 ± 0.087	8.293
14	> 20.243	18.941 ± 0.174	> 17.868	> 1.302	< 1.073	...
15	> 20.243	18.406 ± 0.095	17.407 ± 0.090	> 1.837	0.999 ± 0.131	12.908
16	16.359 ± 0.021	14.866 ± 0.016	14.103 ± 0.023	1.493 ± 0.026	0.763 ± 0.028	9.277
17	> 20.243	18.311 ± 0.111	17.302 ± 0.094	> 1.932	1.009 ± 0.145	13.062
18	off frame	16.840 ± 0.054	16.021 ± 0.031	...	0.819 ± 0.062	10.139
19	> 20.243	18.950 ± 0.127	18.033 ± 0.250	> 1.293	0.917 ± 0.280	11.646
20	18.254 ± 0.063	16.108 ± 0.039	15.040 ± 0.031	2.146 ± 0.074	1.068 ± 0.050	13.970
21	> 20.243	18.337 ± 0.102	...	> 1.906
22	19.462 ± 0.172	17.918 ± 0.103	off frame	1.544 ± 0.200
23	> 20.243	17.784 ± 0.073	16.132 ± 0.064	> 2.459	1.652 ± 0.097	22.954
24	...	17.358 ± 0.155	16.286 ± 0.044	...	1.072 ± 0.161	14.031
25	18.285 ± 0.040	16.777 ± 0.108	16.111 ± 0.075	1.508 ± 0.115	0.666 ± 0.131	7.785
26	17.941 ± 0.060	17.021 ± 0.049	16.861 ± 0.067	0.920 ± 0.077	1.600 ± 0.083	0.000
27	17.872 ± 0.072	16.566 ± 0.106	15.889 ± 0.032	1.306 ± 0.128	0.677 ± 0.111	7.954
28	18.520 ± 0.063	17.318 ± 0.091	16.576 ± 0.059	1.202 ± 0.111	0.742 ± 0.108	8.954
29	17.761 ± 0.028	16.072 ± 0.016	15.291 ± 0.050	1.689 ± 0.032	0.781 ± 0.053	9.554
30	18.387 ± 0.061	15.490 ± 0.041	13.842 ± 0.019	2.897 ± 0.073	1.648 ± 0.045	22.893
31	> 20.243	17.608 ± 0.111	15.911 ± 0.064	> 2.635	1.697 ± 0.128	23.647
32	> 20.243	18.204 ± 0.153	17.107 ± 0.116	> 2.039	1.097 ± 0.192	14.416
33	> 20.243	16.701 ± 0.066	15.406 ± 0.098	> 3.542	1.295 ± 0.118	17.462
34	...	16.972 ± 0.064	15.763 ± 0.081	...	1.209 ± 0.103	16.139
35	> 20.243	18.064 ± 0.139	16.588 ± 0.085	> 2.179	1.476 ± 0.163	20.247
36	16.926 ± 0.019	15.587 ± 0.189	off frame	1.339 ± 0.190
37	17.438 ± 0.046	off frame	off frame
38	18.700 ± 0.153	off frame	off frame
39	18.835 ± 0.088	18.151 ± 0.085	> 17.868	0.684 ± 0.122	< 0.283	...

Table 4. Magnitudes and colors for identified L1582A stars.

Star	J	H	K_s	$J - H$	$H - K_s$	$A_V(K5)$
1	16.187 ± 0.97	14.735 ± 0.048	off frame	1.452 ± 0.108
2	16.837 ± 0.068	14.034 ± 0.034	12.335 ± 0.050	2.803 ± 0.076	1.699 ± 0.060	23.678
3	15.502 ± 0.094	12.289 ± 0.031	10.313 ± 0.035	3.213 ± 0.099	1.976 ± 0.047	27.939
4	> 19.280	17.721 ± 0.153	16.447 ± 0.113	> 1.559	1.274 ± 0.190	17.139
5	14.766 ± 0.028	13.106 ± 0.059	11.840 ± 0.079	1.660 ± 0.065	1.266 ± 0.099	17.016
6	16.162 ± 0.153	14.982 ± 0.138	off frame	1.180 ± 0.206
7	> 19.280	17.059 ± 0.095	15.230 ± 0.117	> 2.221	1.829 ± 0.151	25.678
8	12.070 ± 0.025	11.428 ± 0.020	11.401 ± 0.048	0.642 ± 0.032	0.027 ± 0.072	0.000
9	15.577 ± 0.047	14.511 ± 0.060	13.988 ± 0.112	1.066 ± 0.076	0.523 ± 0.127	5.585
10	17.429 ± 0.078	16.548 ± 0.070	16.293 ± 0.127	0.881 ± 0.105	0.255 ± 0.145	1.462
11	17.426 ± 0.124	17.088 ± 0.114	16.599 ± 0.310	0.338 ± 0.168	0.489 ± 0.330	5.062
12	17.195 ± 0.051	16.433 ± 0.169	15.923 ± 0.162	0.762 ± 0.175	0.510 ± 0.234	5.385
13	17.761 ± 0.156	16.993 ± 0.073	16.424 ± 0.174	0.768 ± 0.172	0.569 ± 0.189	6.292
14	17.831 ± 0.112	> 18.119	> 17.170	< -0.288
15	17.797 ± 0.113	16.727 ± 0.049	16.188 ± 0.128	1.070 ± 0.123	0.539 ± 0.137	5.831
16	off frame	16.803 ± 0.077	16.138 ± 0.069	...	0.665 ± 0.103	7.769
17	> 19.280	17.555 ± 0.102	16.761 ± 0.137	> 1.725	0.794 ± 0.171	9.754

Table 5. Magnitudes and colors for identified L158 stars.

Star	J	H	K_s	$J - H$	$H - K_s$	$A_V(K5)$
1	> 19.999	16.934 ± 0.180	15.266 ± 0.046	> 3.065	1.668 ± 0.184	23.201
2	> 19.999	17.959 ± 0.146	16.250 ± 0.110	> 2.040	1.709 ± 0.183	23.831
3	> 19.999	16.995 ± 0.147	15.509 ± 0.119	> 3.004	1.486 ± 0.189	20.400
4	> 19.999	> 18.577	16.186 ± 0.081	...	> 2.391	34.324
5	17.496 ± 0.190	15.758 ± 0.118	14.807 ± 0.130	1.738 ± 0.224	0.951 ± 0.176	12.170
6	18.343 ± 0.253	17.208 ± 0.340	16.020 ± 0.170	1.135 ± 0.424	1.188 ± 0.380	15.816
7	19.375 ± 0.234	> 18.577	> 17.616	< 0.798
8	12.738 ± 0.038	12.084 ± 0.029	11.859 ± 0.023	0.654 ± 0.048	0.225 ± 0.037	1.000

Table 6. Magnitudes and colors for identified TMC1 stars.

Star	J	H	K_s	$J - H$	$H - K_s$	$A_V(K5)$
1	> 21.396	19.519 ± 0.224	16.574 ± 0.145	> 1.877	2.945 ± 0.267	42.847
2	> 21.396	> 19.889	17.515 ± 0.078
3	> 21.396	18.705 ± 0.143	16.952 ± 0.174	> 2.691	1.753 ± 0.225	24.508
4	> 21.396	18.746 ± 0.146	off frame	> 2.650
5	> 21.396	17.732 ± 0.093	16.086 ± 0.097	> 3.664	1.646 ± 0.134	22.862
6	17.741 ± 0.089	14.622 ± 0.010	12.946 ± 0.016	3.119 ± 0.099	1.676 ± 0.019	23.324
7	> 21.396	18.364 ± 0.073	15.200 ± 0.027	> 3.032	3.164 ± 0.078	46.217
8	> 21.396	18.420 ± 0.217	15.547 ± 0.071	> 2.976	2.873 ± 0.228	41.740
9	> 21.396	18.229 ± 0.093	16.124 ± 0.125	> 3.167	2.105 ± 0.156	29.924
10	> 21.396	18.095 ± 0.114	16.074 ± 0.097	> 3.301	2.021 ± 0.150	28.631
11	20.398 ± 0.111	17.742 ± 0.110	16.763 ± 0.085	2.656 ± 0.156	0.979 ± 0.139	12.600

Table 7. Magnitudes and colors for identified L1696B stars.

Star	J	H	K_s	$J - H$	$H - K_s$	$A_V(K5)$
1	> 18.039	> 18.616	17.619 ± 0.294	...	> 0.997	...
2	> 18.039	> 18.616	17.131 ± 0.215	...	> 1.485	...
3	> 18.039	18.038 ± 0.161	18.168 ± 0.120	> 0.001	-0.130 ± 0.201	...
4	> 18.039	> 18.616	17.773 ± 0.135	...	> 0.843	...
5	> 18.039	17.369 ± 0.209	16.010 ± 0.113	> 0.670	1.359 ± 0.238	18.447
6	> 18.039	> 18.616	17.866 ± 0.101	...	> 0.750	...
7	> 18.039	17.460 ± 0.249	16.086 ± 0.113	> 0.579	1.374 ± 0.273	18.677
8	> 18.039	> 18.616	18.200 ± 0.296	...	> 0.416	...
9	> 18.039	16.623 ± 0.319	14.706 ± 0.024	> 1.416	1.917 ± 0.320	27.031
10	> 18.039	16.763 ± 0.390	14.261 ± 0.025	> 1.276	2.502 ± 0.391	36.032
11	> 18.039	> 18.616	16.402 ± 0.225	...	> 2.214	...
12	> 18.039	18.178 ± 0.167	> 18.263	> -0.139	< -0.085	...

Table 8. Magnitudes and colors for identified L134A stars.

Star	J	H	K_s	$J - H$	$H - K_s$	$A_V(K5)$
1	> 17.947	17.935 ± 0.163	16.550 ± 0.067	> 0.012	1.385 ± 0.176	18.847
2	> 17.947	17.359 ± 0.147	16.126 ± 0.178	> 0.588	1.233 ± 0.231	16.508
3	> 17.947	18.228 ± 0.122	16.485 ± 0.209	> -0.281	1.743 ± 0.242	24.354

Table 9. Magnitudes and colors for identified TMC2 stars. The K_s lower limit is 19.152.

Star	J	H	K_s	$J - H$	$H - K_s$	$A_V(K5)$
1	> 19.329	> 20.113	18.336 ± 0.226	...	> 1.777	...
2	> 19.329	> 20.113	17.751 ± 0.069	...	> 2.362	...
3	> 19.329	18.706 ± 0.183	16.341 ± 0.043	> 0.623	2.365 ± 0.188	33.924
4	> 19.329	...	15.576 ± 0.039
5	> 19.329	> 20.113	17.192 ± 0.082	...	> 2.921	...
6	> 19.329	18.636 ± 0.118	16.955 ± 0.077	> 0.693	1.681 ± 0.141	23.401
7	> 19.329	18.016 ± 0.157	16.128 ± 0.124	> 1.313	1.888 ± 0.200	26.585

Table 10. Magnitudes and colors for identified L183B stars.

Star	J	H	K_s	$J - H$	$H - K_s$	$A_V(K5)$
1	> 18.154	> 18.660	17.115 ± 0.207	...	> 1.545	...
2	> 18.154	> 18.660	17.269 ± 0.152	...	> 1.391	...
3	> 18.154	16.821 ± 0.089	16.028 ± 0.312	> 1.333	0.793 ± 0.324	18.507

Table 11. Five sigma detection limits by filter band and extinction limits for each dense core (see text).

Core	J	H	K_s	$A_V(lim)$
L1709A	20.243	19.262	17.868	45.3
L1582A	19.280	18.119	17.170	34.5
L158	19.999	18.577	17.616	44.5
TMC1	21.396	19.889	19.842	51.3
L1696B	18.039	18.616	18.263	36.8
L134A	17.947	20.152	19.192	40.7
TMC2	19.329	20.113	19.152	43.2
L183B	18.154	18.660	19.151	41.4

Table 12. Mean extinction measures by core.

Core	$\langle A_V(K5) \rangle$
L1709A	12.2
L1582A	11.3
L158	18.7
TMC1	30.3
L1696B	25.0
L134A	19.9
TMC2	28.0
L183B	9.7

Table 13. Estimated core density lower limits and sizes.

Core	n_{tot} (cm^{-3})	M (M_{\odot})	\sqrt{A} (pc)	Polygon Boundary Definition
L1709A	$5.3 \cdot 10^4$	1.3	0.075	15, 17, 23, 30, 31, 34, 35, 29, 25, 24, 20, 15
L1582A	$1.8 \cdot 10^4$	6.0	0.18	3, 7, 8, 9, 10, 11, 12, 13, 15, 16, 17, 3
L158	$8.1 \cdot 10^4$	1.7	0.072	1, 2, 4, 8, 5, 1
TMC1	$1.6 \cdot 10^5$	2.2	0.062	2, 3, 5, 6, 7, 8, 9, 10, 11, 2
TMC2	$5.7 \cdot 10^4$	0.94	0.065	1, 2, 3, 4, 5, 6, 7, 1
L1696B	$5.1 \cdot 10^4$	0.85	0.066	1, 8, 7, 9, 10, 11, 6, 5, 4, 3, 2, 1

Table 14. Results of simple model giving absolute magnitude detection limits to core centers

Core	M_J	M_{det} (M_\odot)
L1709A	10.9	< 0.010
L1582A	8.4	0.020
L158	9.0	0.015
TMC1	7.8	0.030
L1696B	5.4	0.10
L134A	7.7	0.020
TMC2	6.3	0.070
L183B	10.6	< 0.010